

# Pyroeffects on Magneto-Electro-Elastic Sensor patch subjected to thermal load

P. Kondaiah\*<sup>1</sup> and K. Shankar<sup>2a</sup>

<sup>1</sup>Department of Mechanical Engineering, School of Engineering Science, Mahindra École Centrale, Hyderabad, Telangana 500043, India  
<sup>2</sup>Machine Design Section, Department of Mechanical Engineering, Indian Institute of Technology Madras, Chennai 600036, India

(Received February 29, 2016, Revised July 12, 2016, Accepted July 14, 2016)

**Abstract.** The magneto-electro-elastic (MEE) material under thermal environment exhibits pyroelectric and pyromagnetic coefficients resulting in pyroelectric and pyromagnetic effects. The pyroelectric and pyromagnetic effects on the behavior of multiphase MEE sensors bonded on top surface of a mild steel beam under thermal environment is presented in this paper. The aim of the study is to find out how samples having different volume fractions of the multiphase MEE composite behave in sensor applications. This is studied at optimal location on the beam, where the maximum electric and magnetic potentials are induced due to pyroelectric and pyromagnetic effects under clamped-free and clamped-clamped boundary conditions. The sensor which is bonded on the top surface of the beam is modeled using 8-node brick element. The MEE sensor bonded on mild steel beam is subjected to uniform temperature rise of 50K. It is assumed that beam and sensor is perfectly bonded to each other. The maximum pyroelectric and pyromagnetic effects on electric and magnetic potentials are observed when volume fraction is  $v_f=0.2$ . The boundary conditions significantly influence the pyroelectric and pyromagnetic effects on electric and magnetic potentials.

**Keywords:** magneto-electro-elastic sensor; pyroelectric; pyromagnetic; finite element; temperature

## 1. Introduction

Magneto-Electro-Elastic (MEE) composite materials have the ability to generate magnetic, electric and mechanical responses when they experience a thermal stimulus due to its significant coupling between mechanical, electric, magnetic and thermal fields, which are potentially useful in smart or intelligent structure applications. The composite consisting of piezoelectric phase shows a coupling between mechanical and electric fields whereas the piezomagnetic phase shows the coupling between mechanical and magnetic fields. The magnetoelectric coupling effect which is absent in the constituent components is exhibited by this class of material. In addition to this, the pyrocouplings (pyroelectric and pyromagnetic effects) which are not present without a thermal field are also exhibited by this class of MEE materials. These product properties (magnetoelectric, pyroelectric and pyromagnetic effects) are created by coupling of elastic deformations in the piezoelectric and piezomagnetic phases, and the elastic deformations may be induced directly by mechanical loading/temperature gradient or indirectly by an application of electric or magnetic field. The pyrocouplings that exists between the thermoelastic, electric and magnetic fields in  $\text{BaTiO}_3$  -

$\text{CoFe}_2\text{O}_4$  materials provides a means for sensing thermomechanical disturbances from the measurements of induced electrical and magnetic potentials. This unique feature allows magnetic control of electric polarization, electric control of magnetization, and control of electric and magnetic fields with mechanical stress. Due to the exceptional nature of these materials to convert one form of energy into another, find widespread applications in areas like magnetic field probes, acoustic devices, medical ultrasonic imaging, sensors and actuators Wu and Huang (2000). Therefore, these materials with thermal field have attracted significant attention from the scientific community.

Aboudi (2001) has presented the effective moduli of thermo-magneto-electro-elastic composite by employing homogenization method with the assumption that composites have a periodic structure. Sunar *et al.* (2002) has presented finite element modeling of a fully coupled thermopiezomagnetic continuum with the aid of thermodynamic potential. Priya *et al.* (2007) has presented a survey of the recently developed in the area of ME particulate and laminate composites. Nan *et al.* (2008) has presented historical perspective, status, and future directions of multiferroic magnetoelectric composites. Soh and Liu (2005) has presented the recent research advances on the magnetoelectric coupling effect of piezoelectric-piezomagnetic composite materials and their fundamental mechanics issues are reviewed comprehensively. The eight sets of constitutive equations for magneto-electro-elastic solids and the energy functions corresponding to each set of constitutive equations are given. The mathematical properties of the thermodynamic potentials and the relations

\*Corresponding author, Assistant Professor  
E-mail: [kondaiah.iitm@gmail.com](mailto:kondaiah.iitm@gmail.com)

<sup>a</sup>Professor  
E-mail: [skris@iitm.ac.in](mailto:skris@iitm.ac.in)

between the material constants are discussed. Jiang and Li (2007) has presented pyroelectric effect on electric potential of piezoelectric sensor bonded on graphite-epoxy composite beam which is subjected to steady state temperature. Hou *et al.* (2008) have constructed three-dimensional Green's function for a steady point heat source on the surface of a semi-infinite transversely isotropic electro-magneto-thermo-elastic material by using mono-harmonic functions in a very convenient way to use. Pan (2001) derived the exact solution for multilayered electro-magneto-elastic plates using a propagator matrix. The theoretical analysis of a multilayered magneto-electro-thermoelastic hollow cylinder under unsteady and uniform surface heating is presented by Ootao and Ishihara (2011). The exact solution of transient thermal stress problem with the assumption of plane strain state is obtained. Additionally without considering the pyroelectric and pyromagnetic effects, investigated the effects of coupling between magnetic, electric and thermoelastic fields. Biju *et al.* (2011) have presented transient dynamic response for different volume fractions of magneto-electro-elastic sensor bonded on mild steel beam subjected to mechanical loading by using magnetic vector potential approach. Guiffard *et al.* (2010) were studied room temperature magnetic field detection using single piezoelectric disk with a good sensitivity and linear response versus dc magnetic field change. This study validates that ME effect originates from the presence of eddy currents within the metal electrodes of the ceramic, thus yielding radial Lorentz stress which is transduced to the PZT. Kalamkarov *et al.* (2009) have presented the new trends in application of asymptotic homogenization techniques to the analysis of composite materials and thin-walled composite structures, and their effective properties. In addition to review the existing results, they introduced a possibility of analytical solution of the unit cell problems obtained as a result of the homogenization procedure.

Recently, Hadjiloizi *et al.* (2013a) and Hadjiloizi *et al.* (2013b) have presented the effective pyroelectric and pyromagnetic coefficients in micromechanical analysis of magneto-electro-thermo-elastic composite for quasi-static model using the asymptotic homogenization method. The results of this model fully agree with Bravo-Castillero *et al.* (2008). Kalamkarov (2014) has developed micromechanical models by applying asymptotic homogenization technique and obtained analytical formulae for the effective properties to composite materials and thin-walled composite structures.

The fibrous composites consisting of piezomagnetic Cobalt Iron Oxide (CoFe<sub>2</sub>O<sub>4</sub>) matrix reinforced by piezoelectric Barium Titanate (BaTiO<sub>3</sub>) fibers qualify as two phase magneto-electro-elastic material. A sensor made with this two phase magneto-electro-elastic material under thermal stimulus exhibits pyroelectric and pyromagnetic coupling responses. The study of the pyroelectric and pyromagnetic effects on MEE sensor bonded to a mild steel beam using finite element method to account the thermal environment for enhancing the performance of the sensor, appears not to have been investigated to date. Hence the present study is attempted.

## 2. Theoretical formulation

The finite element method is used to analyze pyroeffects (pyroelectric and pyromagnetic) on behavior of magneto-electro-elastic sensor bonded to a mild steel beam. This section presents finite element formulation of the pyroeffects.

### 2.1 Constitutive equations

Multiphase magneto-electro-elastic (MEE) material having piezoelectric phase and piezomagnetic phase under thermal environment exhibits the coupling between mechanical, electrical, magnetic and thermal fields as shown in Fig. 1. The constitutive equations for multiphase magneto-electro-elastic three dimensional solid under thermal environment (temperature field not fully coupled with the magneto-electro-elastic field) in a rectangular Cartesian coordinate system  $(x,y,z)$  are shown in (1). These equations relating stress  $\sigma_j$ , electric displacement  $D_l$ , and magnetic flux density  $B_l$  to strain  $S_k$ , electric field  $E_m$ , magnetic field  $H_m$  and thermal field  $\Theta$ . Linear coupling is assumed between magnetic, electric, thermal and elastic fields (Sunar *et al.* 2002, Gao and Noda 2004).

$$\left. \begin{aligned} \sigma_j &= c_{jk} S_k - e_{mj} E_m - q_{mj} H_m - \gamma_j \Theta \\ D_l &= e_{lk} S_k + \varepsilon_{lm} E_m + m_{lm} H_m + p_l \Theta \\ B_l &= q_{lk} S_k + m_{lm} E_m + \mu_{lm} H_m + \tau_l \Theta \end{aligned} \right\} \quad (1)$$

where  $c_{jk}$ ,  $e_{lk}$ ,  $q_{lk}$  are elastic, piezoelectric, piezomagnetic coefficients respectively and  $\gamma_j$  is the thermal stress coefficient being related with the thermal expansion coefficient  $\beta$  by  $\gamma=c\beta$ .  $\varepsilon_{lm}$ ,  $m_{lm}$ ,  $\mu_{lm}$ ,  $p_l$  and  $\tau_l$  represents respectively the dielectric, magneto-electric, magnetic permeability, pyroelectric and pyromagnetic coefficients. Here  $j, k=1, \dots, 6$  and  $l, m=1, \dots, 3$ . The standard contraction of indices has been used for the elastic constants (i.e.,  $S_4=S_{23}$  etc.).

### 2.2 Finite element formulation

For finite element formulation of a coupled system, the displacements  $\{u\}=\{u_x, u_y, u_z\}^T$ , electrical potential  $\{\phi\}$  and

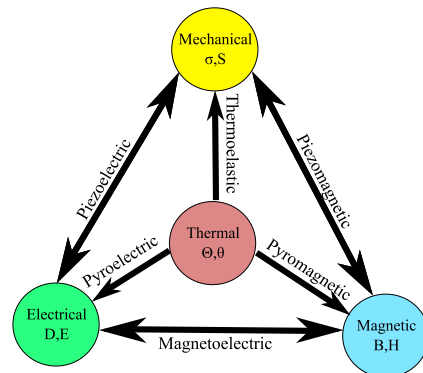


Fig. 1 Schematic diagram showing the complex mechanical, electric, magnetic and thermal coupling (Melvin 2013)

magnetic potential  $\{\psi\}$  within element in terms of suitable shape functions can be written as

$$\begin{aligned} u^e &= [N_u] \{u_i\} \\ \phi^e &= [N_\phi] \{\phi_i\} \\ \psi^e &= [N_\psi] \{\psi_i\} \end{aligned} \quad (2)$$

where the subscripts  $e$  and  $i$  respectively stand for the element and nodes of the element and  $N$  are the shape function matrices whose subscripts denote the associated fields.

The derivation of finite element equations for magneto-electro-thermo-elastic solid by using virtual displacement principle is given by Ganesan *et al.* (2007) and is written in coupled form as

$$\begin{aligned} &\begin{bmatrix} M_{uu}^e & 0 & 0 & 0 \\ 0 & 0 & 0 & 0 \\ 0 & 0 & 0 & 0 \\ 0 & 0 & 0 & 0 \end{bmatrix} \begin{Bmatrix} \ddot{u}^e \\ \ddot{\phi}^e \\ \ddot{\psi}^e \\ \ddot{\Theta}^e \end{Bmatrix} + \begin{bmatrix} 0 & 0 & 0 & -C_{u\Theta}^e \\ 0 & 0 & 0 & 0 \\ 0 & 0 & 0 & 0 \\ C_{\Theta u}^e & -C_{\Theta\phi}^e & -C_{\Theta\psi}^e & C_{\Theta\Theta}^e \end{bmatrix} \begin{Bmatrix} \dot{u}^e \\ \dot{\phi}^e \\ \dot{\psi}^e \\ \dot{\Theta}^e \end{Bmatrix} \\ &+ \begin{bmatrix} K_{uu}^e & K_{u\phi}^e & K_{u\psi}^e & -K_{u\Theta}^e \\ K_{\phi u}^e & -K_{\phi\phi}^e & -K_{\phi\psi}^e & K_{\phi\Theta}^e \\ K_{\psi u}^e & -K_{\psi\phi}^e & -K_{\psi\psi}^e & K_{\psi\Theta}^e \\ 0 & 0 & 0 & K_{\Theta\Theta}^e \end{bmatrix} \begin{Bmatrix} u^e \\ \phi^e \\ \psi^e \\ \Theta^e \end{Bmatrix} = \begin{Bmatrix} f_u^e + T_u^e \\ 0 \\ 0 \\ -T_\Theta^e \end{Bmatrix} \end{aligned} \quad (3)$$

The dynamic behavior of the coupled magneto-electro-thermo-elastic structure is investigated using (3). The prominent contribution of the present work is to formulate the pyroelectric and pyromagnetic effects for an three dimensional magneto-electro-elastic structures under thermal environment using finite element method. To investigate the pyroelectric and pyromagnetic effects, the damping condition is not considered in (3), and is reduced to static case along with the following assumptions,

1. Thermal field of the system is uniform and not fully coupled with the magneto-electro-elastic field, *i.e.*, the magneto-electro-elastic field can be affected by the temperature field through constitutive relations, but the temperature field is not affected by the magneto-electro-elastic field.
2. The mechanical, electric and magnetic fields are fully coupled.
3. The externally applied mechanical force, electric charge and magnetic current are assumed to be zero.

Based on the above assumptions, (3) can be written without considering body and traction forces as

$$\left. \begin{aligned} &[K_{uu}^e] \{u^e\} + [K_{u\phi}^e] \{\phi^e\} + [K_{u\psi}^e] \{\psi^e\} = \{0 + F_{u\Theta}^e\} \\ &[K_{\phi u}^e]^T \{u^e\} - [K_{\phi\phi}^e] \{\phi^e\} - [K_{\phi\psi}^e] \{\psi^e\} = \{0 - F_{\phi\Theta}^e\} \\ &[K_{\psi u}^e]^T \{u^e\} - [K_{\psi\phi}^e]^T \{\phi^e\} - [K_{\psi\psi}^e] \{\psi^e\} = \{0 - F_{\psi\Theta}^e\} \end{aligned} \right\} (4)$$

where  $\{F_{u\Theta}^e\}$ ,  $\{F_{\phi\Theta}^e\}$  and  $\{F_{\psi\Theta}^e\}$  represents the thermal, pyroelectric and pyromagnetic load vectors respectively, and these are explained in Section 2.2.1. (Note: The negative signs of  $\{F_{\phi\Theta}^e\}$  and  $\{F_{\psi\Theta}^e\}$  in (4) are taken care of by pyroelectric and pyromagnetic properties in Table 1).

The matrix  $K_{u\phi}^e$  is element stiffness matrix due to piezoelectric-mechanical coupling effect, and  $K_{u\psi}^e$  is element stiffness matrix due to piezomagnetic-mechanical coupling effect, and  $K_{\phi\psi}^e$  is element stiffness matrix due to magneto-electric coupling effect.  $K_{u\Theta}^e$ ,  $K_{\phi\Theta}^e$  and  $K_{\psi\Theta}^e$  are element stiffness matrices due to thermal-mechanical, thermal-electrical and thermal-magnetic coupling effects respectively. The matrices  $K_{uu}^e$ ,  $K_{\phi\phi}^e$  and  $K_{\psi\psi}^e$  are element stiffness matrices due to mechanical, electrical and magnetic fields respectively.

### 2.2.1 Evaluation of elemental matrices

The different elemental matrices of Eq. (4) for magneto-electro-elastic solid are further defined as

$$\begin{aligned} [K_{uu}^e] &= \int_v [B_u]^T [c] [B_u] dv; \\ [K_{u\phi}^e] &= \int_v [B_u]^T [e] [B_\phi] dv; \\ [K_{u\psi}^e] &= \int_v [B_u]^T [q] [B_\psi] dv; \\ [K_{\phi\psi}^e] &= \int_v [B_\phi]^T [m] [B_\psi] dv; \\ [K_{\phi\phi}^e] &= \int_v [B_\phi]^T [\varepsilon] [B_\phi] dv; \\ [K_{\psi\psi}^e] &= \int_v [B_\psi]^T [\mu] [B_\psi] dv \end{aligned}$$

In the present study, for a specified uniform temperature rise ( $\Theta$ ), the thermal load, equivalent pyroelectric load (electric load generated due to temperature) and pyromagnetic load (magnetic load generated due to temperature) terms are calculated, and applied as external loads in the system equations given in (4). These can be solved for displacements, electric potential and magnetic potential. These external vectors used in the system equations are given as follows

$$\{F_{u\Theta}^e\} = [K_{u\Theta}^e] \{\Theta\} = \int_v [B_u]^T [c] [\beta] \Theta dv \quad (5)$$

where  $\{F_{u\Theta}^e\}$  is the thermal load vector and is governed as a direct effect on displacements, and indirect effect on electric and magnetic potentials through constitutive equations

$$\{F_{\phi\Theta}^e\} = [K_{\phi\Theta}^e] \{\Theta\} = \int_v [B_\phi]^T [p] \Theta dv \quad (6)$$

where  $\{F_{\phi\Theta}^e\}$  is the pyroelectric load vector and is governed as a direct effect on electric potential, and indirect effect on magnetic potential and displacement through constitutive equations

$$\{F_{\psi\Theta}^e\} = [K_{\psi\Theta}^e] \{\Theta\} = \int_v [B_\psi]^T [\tau] \Theta dv \quad (7)$$

where  $\{F_{\psi\Theta}^e\}$  is the pyromagnetic load vector and it is governed as a direct effect on magnetic potential, and indirect effect on electric potential and displacements through constitutive equations.

The coupled formation of Eq. (4) can be written as

$$\begin{bmatrix} K_{uu} & K_{u\phi} & K_{u\psi} \\ K_{\phi u} & -K_{\phi\phi} & -K_{\phi\psi} \\ K_{\psi u} & -K_{\psi\phi} & -K_{\psi\psi} \end{bmatrix} \begin{Bmatrix} u \\ \phi \\ \psi \end{Bmatrix} = \begin{Bmatrix} F_{u\Theta} \\ F_{\phi\Theta} \\ F_{\psi\Theta} \end{Bmatrix} \quad (8)$$

### 3. Numerical modelling

The finite element method is used to analyze pyroelectric and pyromagnetic effects on behavior of magneto-electro-elastic sensor bonded to a mild steel beam subjected to uniform temperature rise of 50K. The purpose of the sensor is to measure electric and magnetic response to applied thermal environment. The main objective of the present work is to study the influence of different volume fractions of composite and the influence of boundary condition on behavior of MEE sensor due to pyroelectric and pyromagnetic effects. The sensor bonded on top surface of the beam at optimal location (clamped end) is considered based on optimal sensor placement as discussed in Section 3.2. The advantage of considering optimal sensor placement study is that there is no need to analyze the sensor behavior at selective locations such as clamped end, intermediate location, free end, etc.

The multiphase MEE sensor is made of piezomagnetic (CoFe<sub>2</sub>O<sub>4</sub>) matrix reinforced by piezoelectric (BaTiO<sub>3</sub>) material for different volume fractions  $v_f=0.0$  to  $v_f=1.0$  in steps of 0.2. The  $v_f=1.0$  corresponds to pure piezoelectric material and  $v_f=0.0$  corresponds to pure piezomagnetic material.

The pyroelectric effect can manifest in MEE sensor through the pyroelectric load (Refer Eq. (6)) when the beam is subjected to uniform temperature rise. Similarly, the pyromagnetic effect can manifest through the pyromagnetic load (Refer Eq. (7)). Influence of both the pyroelectric and pyromagnetic loads are called direct effect on electric and magnetic potentials respectively. Indirectly, the values of electric and magnetic potentials due to thermal load (Refer Eq. (5)) can be developed through constitutive equations (Refer Eq. (1)). This is called indirect effect on electric and magnetic potentials (Refer Section 2.2.1). Whereas in the case of displacement, it is vice-versa.

Fig. 2 shows the finite element discretization model of MEE sensor placed on top surface of clamped-free mild steel beam in rectangular Cartesian coordinate system ( $x, y, z$ ) along with finite element discretization model in natural coordinate ( $\xi, \eta, \tau$ ) system. The dimensions of 3D base beam used for analysis are 0.3 m × 0.02 m × 0.01 m. The dimensions of sensor are 0.02 m × 0.002 m × 0.01 m. An optimum mesh size is chosen which make the results within acceptable limits. The arrangement consists of one electrode from the beam which is grounded and the other electrode which is kept on the top of the sensor patch. The magnetic potentials are assumed to be zero at the clamped end. To study the pyroelectric and pyromagnetic effects on bonded MEE sensor, the results are compared with conventional approach which presumed as without considering pyroelectric and pyromagnetic loads or in other words, the coefficients  $\gamma \neq 0$ ,  $p=0$  and  $\tau=0$ .

Table 1 Material properties of PZT5A and different volume fraction of multiphase MEE BaTiO<sub>3</sub>-CoFe<sub>2</sub>O<sub>4</sub> (Aboudi 2001, Hadjiloizi *et al.* 2013a, b, Chen *et al.* 2007, Biju *et al.* 2011, Pan 2002, Pan and Chen 2015)

	0.0 $v_f$	0.2 $v_f$	0.4 $v_f$	0.6 $v_f$	0.8 $v_f$	1.0 $v_f$	PZT-5A
Elastic constants							
$c_{11}=c_{22}$	286	250	225	200	175	166	99.2
$c_{12}$	173	146	125	110	100	77	54
$c_{13}=c_{23}$	170	145	125	110	100	78	50.8
$c_{33}$	269.5	240	220	190	170	162	86.9
$c_{44}=c_{55}$	45.3	45	45	45	50	43	21.1
Piezoelectric constants							
$e_{31}=e_{32}$	0	-2.0	-3.0	-3.5	-4.0	-4.4	-7.2
$e_{33}$	0	4.0	7.0	11.0	14.0	18.6	15.1
$e_{24}=e_{15}$	0	0	0	0	0	11.6	12.3
Dielectric constants							
$\epsilon_{11}=\epsilon_{22}$	0.08	0.33	0.8	0.9	1.0	11.2	1.53
$\epsilon_{33}$	0.093	2.5	5.0	7.5	10.0	12.6	1.5
Magnetic permeability constants							
$\mu_{11}=\mu_{22}$	-5.9	-3.9	-2.5	-1.5	-0.8	0.05	0
$\mu_{33}$	1.57	1.33	1.0	0.75	0.5	0.1	0
Piezomagnetic constant							
$q_{31}=q_{32}$	580	410	300	200	100	0	0
$q_{33}$	700	550	380	260	120	0	0
$q_{24}=q_{15}$	560	340	220	180	80	0	0
Magnetolectric constants							
$m_{11}=m_{22}$	0	2.8	4.8	6.0	6.8	0	0
$m_{33}$	0	2000	2750	2500	1500	0	0
Pyroelectric constants							
$p_2$	0	-3.5	-6.5	-9	-10.8	0	
Pyromagnetic constants							
$\tau_2$	0	-36	-28	-18	-8.5	0	0
Thermal expansion coefficient							
$\beta_{11}=\beta_{22}$	10	10.8	11.8	12.9	14.1	15.7	1.5
$\beta_{33}$	10	9.3	8.6	7.8	7.2	6.4	1.5
Density							
$\rho$	5300	5400	5500	5600	5700	5800	7750

$c_{ij}$  in N/m<sup>2</sup>,  $e_{ij}$  in C/m<sup>2</sup>,  $\epsilon_{ij}$  in 10<sup>-9</sup> C<sup>2</sup>/N m<sup>2</sup> or 10<sup>-9</sup> C/V m,  $q_{ij}$  in N/A m,  $\mu_{ij}$  in 10<sup>-4</sup> N s<sup>2</sup>/C<sup>2</sup>,  $m_{ij}$  in 10<sup>-12</sup> N s/V C,  $p_i$  in 10<sup>-7</sup> C/m<sup>2</sup> K,  $\tau_i$  in 10<sup>-5</sup> C/m<sup>2</sup> K,  $\beta_{ij}$  in 10<sup>-6</sup> 1/K,  $\rho$  in kg/m<sup>3</sup>

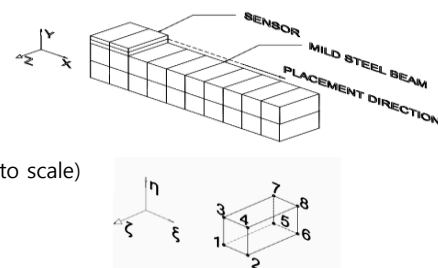


Fig. 2 Initial position of MEE sensor bonded on mild steel beam with Finite Element discretization

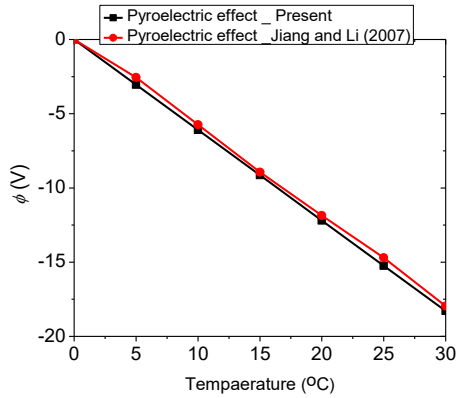


Fig. 3 Validation of pyroelectric effect on electric potential

### 3.1 Validation of the proposed formulation

A computer code has been developed to study the pyroelectric and pyromagnetic effects on the behavior of bonded MEE sensor under clamped-free and clamped-clamped boundary conditions. The pyroelectric effect on electric potential of piezoelectric sensor bonded on graphite-epoxy composite beam which is subjected to steady state temperature presented by Jiang and Li (2007) is compared with the present code. Fig. 3 shows the validation of pyroelectric effect on electric potential ( $\phi$ ) of the sensor by Jiang and Li (2007) in comparison with present formulation. It is seen that the results obtained by Jiang and Li (2007) is in close agreement with present formulation.

The commercial finite element package ANSYS was also used for validating the methodology adopted. The piezomagnetic material can be modeled using ANSYS since the constitutive relations as well as the governing field equations (if free currents and transient effects are neglected) are of identical format with piezoelectric materials. Since ANSYS does not explicitly contain piezomagnetic relationships, it is unable to model fully coupled MEE material which is combined response of both piezoelectric and piezomagnetic material model simultaneously. Thus commercial finite element package ANSYS was used for validating the methodology adopted for solution procedure. Fig. 4 shows the axial displacement component ( $u_x$ ) along the length on the top surface of

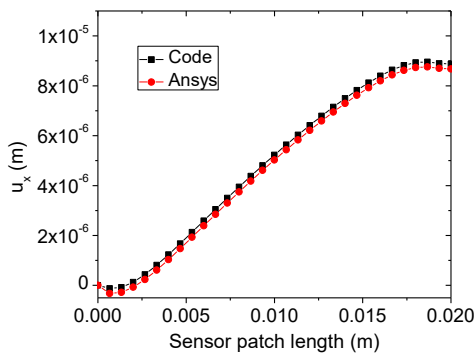
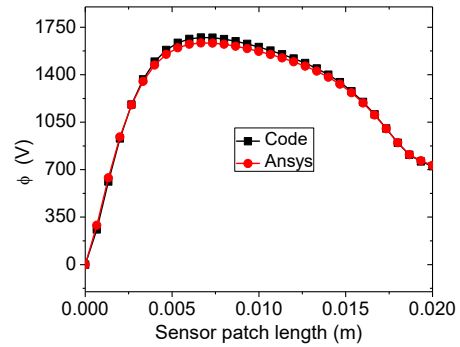
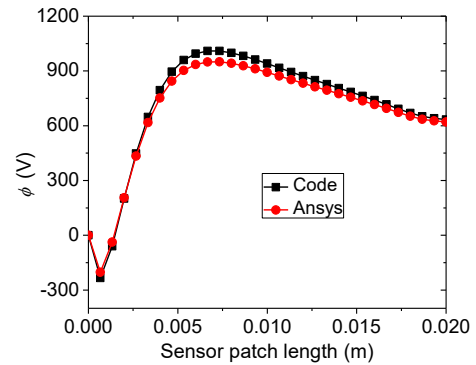


Fig. 4 Validation of axial displacement (clamped-free boundary condition)



(a)



(b)

Fig. 5 Validation of electric potential under (a) clamped-free and (b) clamped-clamped boundary conditions

piezoelectric sensor bonded on mild steel beam under clamped-free boundary condition. And Fig. 5 shows the electric potential of the sensor under clamped-free as well as clamped-clamped boundary conditions. The results obtained by ANSYS are found to be in good agreement with the present formulation.

### 3.2 Optimal Placement of MEE Sensor

The optimal placement of MEE sensor on top surface of the mild steel beam for maximum electric potential due to pyroelectric and pyromagnetic effects is studied. The optimal location of MEE sensor on top surface of the beam is carried out by implementing auto-mesh generation at different positions along the length of the beam under clamped-free as well as clamped-clamped boundary conditions. In finite element formulation of placing a sensor on beam need to generate common nodes at interface between sensor and beam. The generation of common nodes at interface of sensor and beam need to repeat for placement of sensor at different positions along the length of the beam. In auto-mesh generation, the computer code will regenerate interface nodes between sensor and beam in every placement of sensor on beam at different positions along the length of the beam.

The auto-mesh generation regenerates mesh for sensor and base structure with connectivity at interface using the code incorporating the pyroelectric and pyromagnetic effects studied in this paper. It calculates the stiffness

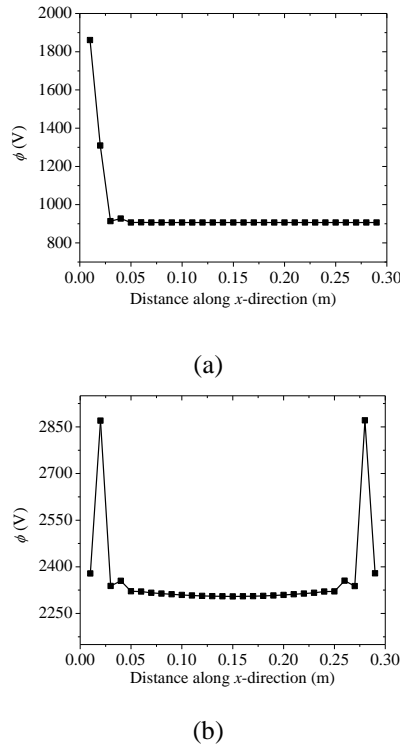


Fig. 6 Electric potential ( $\phi$ ) corresponding to the position of MEE sensor on top surface of mild steel beam under (a) clamped-free and (b) clamped-clamped boundary conditions

matrix and load vector at every location on the structure where the sensor is placed. The study is carried out for volume fraction  $v_f=0.4$  of BaTiO<sub>3</sub>. It is assumed that the electric potential of the sensor is not arrested at clamped end. Fig. 6 shows the electric potential ( $\phi$ ) corresponding to the position of the MEE sensor on top surface of mild steel beam under both the boundary conditions. It is observed that the electric potential is maximum near the clamped end of the beam under both clamped-free and clamped-clamped boundary conditions. This optimal location of the sensor on the beam (clamped end) is considered to carry out the objective which discussed in Section 3 under both the boundary conditions. Based on this two cases are considered, namely *Case-I* (clamped-free boundary condition with sensor at optimal location) and *Case-II* (clamped-clamped boundary condition with sensor at optimal location) which are discussed in detail in Section 4.

#### 4. Results and discussion

##### 4.1 Case-I: Clamped-Free Boundary Condition with Sensor at Optimal Location

The main objective of this section is to study the influence of different volume fractions of composite and the influence of boundary condition on behavior of MEE sensor due to pyroelectric and pyromagnetic effects. The sensor bonded on top surface of the beam at optimal location (clamped end) is considered based on optimal sensor

placement as discussed in Section 3.2.

The variation of axial ( $u_x$ ), transverse y-direction ( $u_y$ ), transverse z-direction ( $u_z$ ) displacement components, and electric and magnetic potentials along the length on top surface of the sensor patch are shown in Fig. 7(a)-(e) respectively. It is observed that the axial displacement component is varying linearly and is maximum at the free end. The transverse y-direction and z-direction displacement components are maximum near the clamped end and almost remain constant along the length of the sensor for all volume fractions of BaTiO<sub>3</sub>. The displacement components are not affected by pyroelectric and pyromagnetic effects.

The magnitude of electric potential is observed to be maximum for volume fraction  $v_f=0.2$  (Fig. 7(d)) and is zero for volume fraction  $v_f=0.0$  (pure piezomagnetic phase). The magnitude of electric potential is maximum near the

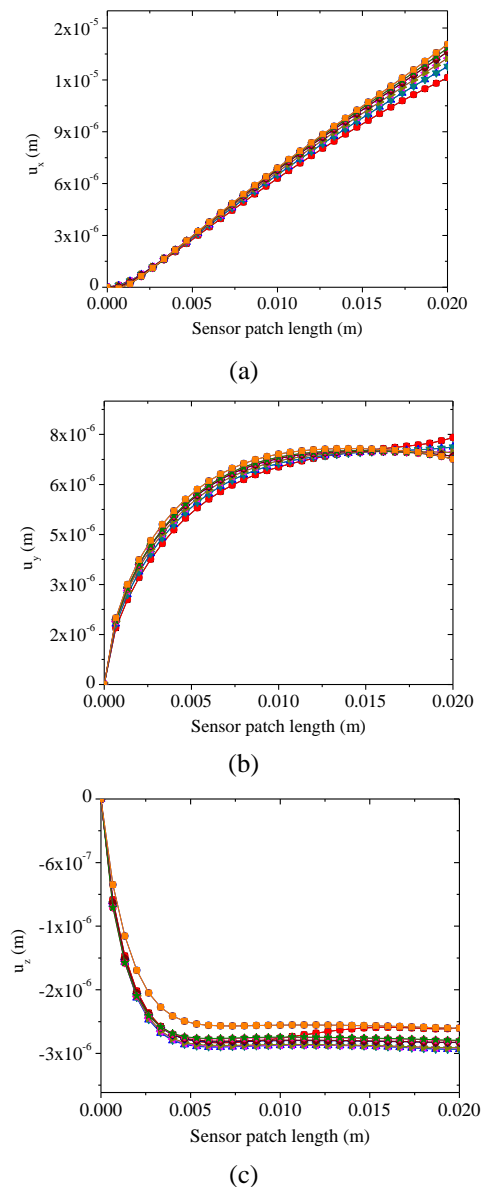
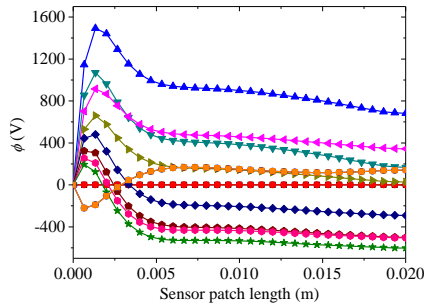
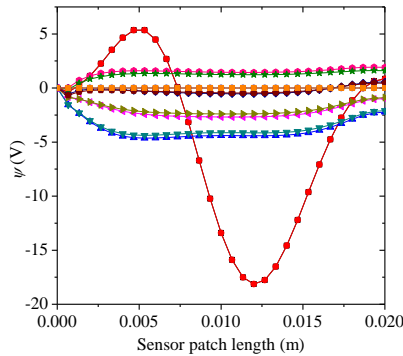


Fig. 7 Variation of (a) axial, (b) transverse y-direction, (c) transverse z-direction displacement components, and (d) electric and (e) magnetic potentials on top surface of the sensor patch (C-F boundary condition)



(d)



(e)

Legend (Fig. 7(a)-(e))

- with pyroelectric and pyromagnetic\_0.0vf
- conventional approach\_0.0vf
- ▲ with pyroelectric and pyromagnetic\_0.2vf
- ▼ conventional approach\_0.2vf
- ◆ with pyroelectric and pyromagnetic\_0.4vf
- ▽ conventional approach\_0.4vf
- ◇ with pyroelectric and pyromagnetic\_0.6vf
- ◇ conventional approach\_0.6vf
- ◆ with pyroelectric and pyromagnetic\_0.8vf
- ▽ conventional approach\_0.8vf
- ◇ with pyroelectric and pyromagnetic\_1.0vf
- ▽ conventional approach\_1.0vf

Fig. 7 Continued

clamped end and decreases along the length of the sensor for all volume fractions. There is no change in the sign of the electric potential curve along the length of the sensor for volume fraction  $v_f=0.2$  and  $v_f=0.4$ . It is also observed that there is a change in sign of the curve from positive to negative for  $v_f=0.6$  and  $v_f=0.8$ , whereas the curve shows an opposite change for volume fraction  $v_f=1.0$ . This change in sign of MEE sensor potential is very important in designing switchers/sensors.

Unlike the displacement components, electric potential is affected by the pyroelectric and pyromagnetic effects. The variation of electric potential with pyroelectric and pyromagnetic effects follows the same trend as the conventional approach. There is an increase in the electric potential due to pyroelectric and pyromagnetic effects as compared to conventional approach. The maximum pyroelectric and pyromagnetic effects on electric potential is observed for the volume fraction  $v_f=0.2$  (Fig. 7(d)), and is minimum for  $v_f=0.8$  whereas no effect is observed for  $v_f=0.0$  and  $v_f=1.0$ . The difference in amplitude can be attributed to the induced strain because of the high elastic constants for  $v_f=0.2$ .

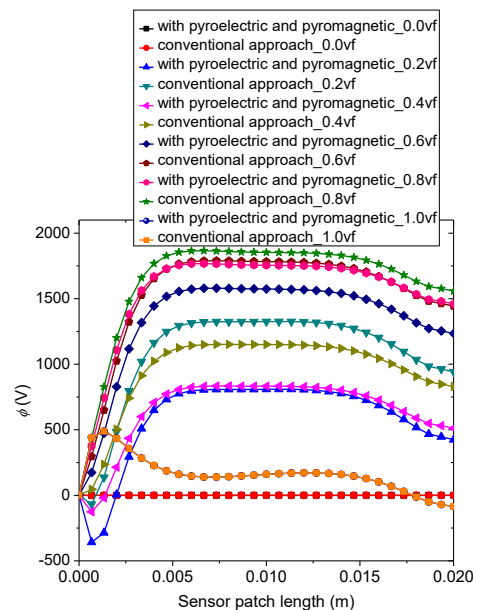
The magnitude of magnetic potential is maximum for

volume fraction  $v_f=0.0$  (Fig. 7(e)) and is zero for  $v_f=1.0$  (pure piezoelectric phase). A sinusoidal variation is observed for  $v_f=0.0$ . There is no change in the sign of the magnetic potential curve along the length of the sensor for volume fraction  $v_f=0.2$ ,  $v_f=0.4$  and  $v_f=0.8$ . It is also observed that there is a change in sign of the curve from negative to positive for  $v_f=0.6$ . The variation of magnetic potential with pyroelectric and pyromagnetic effects follows the same trend as the conventional approach. There is an increase in the magnetic potential due to pyroelectric and pyromagnetic effects as compared to the conventional approach. The maximum effects on magnetic potential is observed for the volume fraction  $v_f=0.2$  (Fig. 7(e)), and is minimum for  $v_f=0.6$ , whereas no effect is observed for  $v_f=0.0$  and  $v_f=1.0$ .

#### 4.2 Case-II: Clamped-Clamped boundary condition with sensor at optimal location

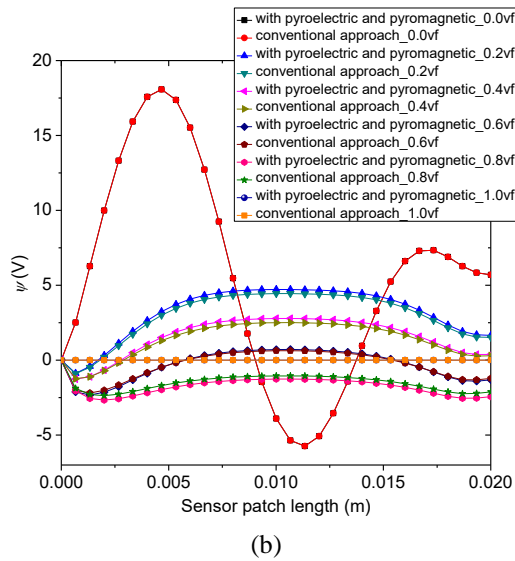
Fig. 8(a) and 8(b) shows the variation of electrical ( $\phi$ ) and magnetic potential ( $\psi$ ) on top surface along the length of the sensor patch. Similar observations are noticed for displacement components in the clamped-clamped boundary condition as in case of clamped free boundary condition. Hence the displacement components are not shown.

The magnitude of electric potential is maximum near the clamped end and remains constant in between and reduces at the free end along the length of the sensor patch for all volume fractions. The magnitude of electric potential is maximum for  $v_f=0.8$  (Fig. 8(a)) and is zero for  $v_f=0.0$  (pure piezomagnetic phase). There is a change in sign of the curve from negative to positive for  $v_f=0.4$ . The change in sign of the curve from negative to positive is also observed



(a)

Fig. 8 Variation of (a) electric and (b) magnetic potentials on top surface of the sensor patch (C-C boundary condition)

(b)  
Fig. 8 Continued

in the conventional approach for  $v_f=0.2$ . Whereas the curve shows an opposite change for volume fraction  $v_f=1.0$ . There is no change in the sign of the electric potential curve along the length of the sensor patch for all other volume fractions.

The variation of electric potential with pyroelectric and pyromagnetic effects follows the same trend as the conventional approach. Unlike the clamped free boundary condition, there is an increase in the electric potential due to pyroelectric and pyromagnetic effects. This feature is consistent with recent modeling results as presented by Pan and Wang (2009) for the ME effect study. The maximum pyroelectric and pyromagnetic effects on electric potential is observed for the volume fraction  $v_f=0.2$  (Fig. 8(a)), and is minimum for  $v_f=0.8$ , whereas no effect is observed for  $v_f=0.0$  and  $v_f=1.0$  which is similar to the clamped free case.

The magnetic potential is found to be following a wavelike path with a high amplitude for  $v_f=0.0$  (Fig. 8(b)) and low amplitude for  $v_f=0.6$ . The other observations are found to be in line with the clamped free case except that the curves try to maintain a symmetric variation along the length of the sensor.

## 5. Conclusions

The pyroelectric and pyromagnetic effects on the behavior of a magneto-electro-elastic sensor bonded to a mild steel beam is evaluated using the finite element method. The pyroelectric and pyromagnetic loads which are generated from an applied uniform temperature rise are used to study the pyroeffects to account for the thermal environment. It is observed that,

- The displacement components of the sensor patch are not affected by the pyroelectric and pyromagnetic effects for all volume fractions of the composite.
- Except for the volume fractions  $v_f=0.0$  and  $v_f=1.0$ , all other volume fractions of the composite exhibit the pyroelectric and pyromagnetic effects on electric and magnetic potentials. The maximum pyroeffects on

electric and magnetic potentials are observed when the volume fraction is  $v_f=0.2$  for clamped-free as well as clamped-clamped boundary conditions. This can be attributed to the induced strain because of the high elastic constants for  $v_f=0.2$ .

- The pyroelectric and pyromagnetic effects on electric potential are maximum in the clamped-clamped boundary condition than the clamped-free boundary condition. The reason for the lower magnitude may be due to lower stress (clamped-free) when compared to the clamped-clamped boundary condition.

- The near clamped end is the optimal location of the sensor on the beam for obtaining maximum electric potential due to pyroelectric and pyromagnetic effects.

These studies will be very significant in enhancing the sensitivity of MEE sensors' electric and magnetic potentials.

## References

- Aboudi, J. (2001), "Micromechanical analysis of fully coupled electro-magneto-thermo-elastic multiphase composites", *Smart Mater. Struct.*, **10**(5), 867-877.
- Biju, B., Ganesan, N. and Shankar, K. (2011), "Dynamic response of multiphase magneto-electro-elastic sensors using 3D magnetic vector potential approach", *IEEE Sens. J.*, **11**(9), 2169-2176.
- Bravo-Castillero, J., Rodriguez-Ramos, R., Mechkour, H., Otero, J. and Sabina, F.J. (2008), "Homogenization of magneto-electro-elastic multilaminated materials", *Q. J. Mech. Appl. Math.*, **61**(3), 311-322.
- Chen, J., Pan, E. and Chen, H. (2007), "Wave propagation in magneto-electro-elastic multilayered plates", *Int. J. Solids Struct.*, **44**(3), 1073-1085.
- Ganesan, N., Kumaravel, A. and Raju Sethuraman (2007), "Finite element modeling of a layered, multiphase magneto-electro-elastic cylinder subjected to an axisymmetric temperature distribution", *J. Mech. Mater. Struct.*, **2**(4), 655-674.
- Gao, C.F. and Noda, N. (2004), "Thermal-induced interfacial cracking on magneto-electro-elastic materials", *Int. Eng. Sci.*, **42**(13), 1347-1360.
- Guiffard B., Zhang, J.W., Guyomar, D., Garbuio, L., Cottinet, P.J. and Belouadah, R. (2010), "Magnetic field sensing with a single piezoelectric ceramic disk: Experiments and modeling", *J. Appl. Phys.*, **108**(9), 094901.
- Hadjiloizi, D.A., Georgiades, A.V., Kalamkarov, A.L. and Jothi, S. (2013a), "Micromechanical modeling of Piezo-Magneto-Thermo-Elastic composite structures: Part I - Theory", *Eur. J. Mech. A. Solids*, **39**, 298-312.
- Hadjiloizi, D.A., Georgiades, A.V., Kalamkarov, A.L. and Jothi, S. (2013b), "Micromechanical modeling of Piezo-Magneto-Thermo-Elastic composite structures: Part II - Theory", *Eur. J. Mech. A. Solids*, **39**, 313-327.
- Hou, P.F., Andrew-Y.T. Leung and Hao-Jiang, Ding (2008), "A point heat source on the surface of a semi-infinite transversely isotropic electro-magneto-thermo-elastic material", *Int. J. Eng. Sci.*, **46**(3), 273-285.
- Jiang, J.P. and Li, D.X. (2007), "A new finite element model for piezothermoelastic composite beam", *J. Sound Vib.*, **306**(3), 849-864.
- Kalamkarov, A.L., I. Andrianov and Vladyslav V. Danishevskyy (2009), "Asymptotic homogenization of composite materials and structures", *Appl. Mech. Rev.*, **62**(3), 030802.

- Kalamkarov, A.L. (2014), "Asymptotic homogenization method and micromechanical models for composite materials and thin-walled composite structures", Chapter 1 in *Mathematical Methods and Models in Composites*, Imperial College Press, London.
- Melvin M. Vopson (2013), "Theory of giant-caloric effects in multiferroic materials", *J. Phys. D: Appl. Phys.*, **46**(34), 345304.
- Nan, C.W., Bichurin, M.I., Shuxiang Dong, Viehland, D. and Srinivasan, G. (2008), "Multiferroic magnetoelectric composites: Historical perspective, status, and future directions", *J. Appl. Phys.*, **103**(3), 1-35.
- Ootao, Y. and Ishihara, M. (2011), "Exact solution of transient thermal stress problem of the multilayered magneto-electro-thermoelastic hollow cylinder", *J. Solid Mech. Mater. Eng.*, **5**(2), 90-103.
- Pan, E. (2001), "Exact solution for simply supported and multilayered magneto-electro-elastic plates", *J. Appl. Mech.*, ASME, **68**(4), 608-618.
- Pan, E. and Wang, R. (2009), "Effects of geometric size and mechanical boundary conditions on magnetoelectric coupling in multiferroic composites", *J. Phys. D: Appl. Phys.*, **42**(24), 245503.
- Pan, E. (2002), "Three-dimensional Green's functions in anisotropic magneto-electro-elastic biomaterials", *J. Appl. Math. Phys. (ZAMP)*, **53**(5), 815-838.
- Pan, E. and Chen, W.Q. (2015), *Static Green's Functions in Anisotropic Media*, Cambridge University Press, New York, USA.
- Priya, S., Rashed Islam, Shuxiang Dong and D. Viehland (2007), "Recent advancements in magnetoelectric particulate and laminate composites", *J. Electroceram*, **19**(1), 147-164.
- Soh, A.K. and Liu, J.X. (2005), "On the constitutive equations of magneto-electroelastic solids", *J. Intel. Mater. Syst. Struct.*, **16**(7-8), 597-602.
- Sunar, M., Al-Garni, A.Z., Ali, M.H. and Kahraman, R. (2002), "Finite element modeling of thermopiezomagnetic smart structures", *AIAA J.*, **40**(9), 1846-1851.
- Wu, T.L. and Huang, J.H. (2000), "Closed-form solutions for the magneto-electric coupling coefficients in Fibrous composites with piezoelectric and piezomagnetic phases", *Int. J. Solid. Struct.*, **37**(21), 2981-3009.